Diffusing-wave spectroscopy with dynamic contrast variation: disentangling the effects of blood flow and extravascular tissue shearing on signals from deep tissue

Markus Ninck, Markus Untenberger, and Thomas Gisler
Universität Konstanz, Fachbereich Physik, 78457 Konstanz, Germany
thomas.gisler@uni-konstanz.de

Abstract: We investigate the effects of blood flow and extravascular tissue shearing on diffusing-wave spectroscopy (DWS) signals from deep tissue, using an *ex vivo* porcine kidney model perfused artificially at controlled arterial pressure and flow. Temporal autocorrelation functions $g^{(1)}(\tau)$ of the multiply scattered light field show a decay which is described by diffusion for constant flow, with a diffusion coefficient scaling linearly with volume flow rate. Replacing blood by a non-scattering fluid reveals a flow-independent background dynamics of the extravascular tissue. For a sinusoidally driven perfusion, field autocorrelation functions $g^{(1)}(\tau,t')$ depend on the phase t' within the pulsation cycle and are approximately described by diffusion. The effective diffusion coefficient $D_{\mathrm{eff}}(t')$ is modulated at the driving frequency in the presence of blood, showing coupling with flow rate; in the absence of blood, $D_{\mathrm{eff}}(t')$ is modulated at twice the driving frequency, indicating shearing of extravascular tissue as the origin of the DWS signal. For both constant and pulsatile flow the contribution of extravascular tissue shearing to the DWS signal is small.

OCIS codes: (030.6140) Speckle; (170.0170) Medical optics and biotechnology; (170.1470) Blood or tissue constituent monitoring; (170.5280) Photon migration; (290.1990) Diffusion; (290.1350) Backscattering; (290.4210) Multiple Scattering; (290.7050) Turbid media

References and links

1. G. Maret and P. E. Wolf, "Multiple light scattering from disordered media: The effect of Brownian motion of scatterers," Z. Phys. B **65**, 409–413 (1987).
2. D. J. Pine, D. A. Weitz, P. M. Chaikin, and E. Herbolzheimer, "Diffusing-wave spectroscopy," Phys. Rev. Lett. **60**, 1134–1137 (1988).
3. T. Durduran, G. Yu, M. G. Burnett, J. A. Detre, J. H. Greenberg, J. Wang, C. Zhou, and A. G. Yodh, "Diffuse optical measurement of blood flow, blood oxygenation, and metabolism in a human brain during sensorimotor cortex activation," Opt. Lett. **29**, 1766–1768 (2004).
4. J. Li, G. Dietsche, D. Iftime, S. E. Skipetrov, G. Maret, T. Elbert, B. Rockstroh, and T. Gisler, "Non-invasive detection of functional brain activity with near-infrared diffusing-wave spectroscopy," J. Biomed. Opt. **10**, 044002 (2005).
5. F. Jaillon, S. E. Skipetrov, J. Li, G. Dietsche, G. Maret, and T. Gisler, "Diffusing-wave spectroscopy from head-like tissue phantoms: influence of a non-scattering layer," Opt. Express **14**, 10181–10194 (2006).
6. J. Li, M. Ninck, L. Koban, T. Elbert, J. Kissler, and T. Gisler, "Transient functional blood flow change in the human brain measured non-invasively by diffusing-wave spectroscopy," Opt. Lett. **33**, 2233–2235 (2008).

#136026 - $15.00 USD Received 1 Oct 2010; revised 12 Nov 2010; accepted 20 Nov 2010; published 29 Nov 2010

7. L. Koban, M. Ninck, J. Li, T. Gisler, and J. Kissler, "Processing of emotional words measured simultaneously with steady-state visually evoked potentials and near-infrared diffusing wave spectroscopy," BMC Neurosci. **11**, 85 (2010).
8. G. Yu, T. F. Floyd, T. Durduran, C. Zhou, J. Wang, J. A. Detre, and A. G. Yodh, "Validation of diffuse correlation spectroscopy for muscle blood flow with concurrent arterial spin labeled perfusion MRI," Opt. Express **15**, 1064–1075 (2007).
9. T. Durduran, C. Zhou, E. M. Buckley, M. N. Kim, R. Choe, J. W. Gaynor, T. L. Spray, S. M. Durning, S. E. Mason, L. M. Montenegro, S. C. Nicolson, R. A. Zimmerman, M. E. Putt, J. Wang, J. H. Greenberg, J. A. Detre, A. G. Yodh, and D. J. Licht, "Optical measurement of cerebral hemodynamics and oxygen metabolism in neonates with congenital heart defects," J. Biomed. Opt. **15**, 037004 (2010).
10. S. A. Carp, G. P. Dai, D. A. Boas, M. A. Franceschini, and Y. R. Kim, "Validation of diffuse correlation spectroscopy measurements of rodent cerebral blood flow with simultaneous arterial spin labeling MRI; towards MRI-optical continuous cerebral metabolic monitoring," Biomed. Opt. Express **1**, 553–565 (2010).
11. M. N. Kim, T. Durduran, S. Frangos, B. L. Edlow, E. M. Buckley, H. E. Moss, C. Zhou, G. Yu, R. Choe, E. Maloney-Wilensky, R. L. Wolf, M. S. Grady, J. H. Greenberg, J. M. Levine, A. G. Yodh, J. A. Detre, and W. A. Kofke, "Noninvasive measurement of cerebral blood flow and blood oxygenation using near-infrared and diffuse correlation spectroscopies in critically brain-injured adults," Neurocrit. Care **12**, 173–180 (2010).
12. C. Zhou, S. A. Eucker, T. Durduran, G. Yu, J. Ralston, S. H. Friess, R. N. Ichord, S. S. Margulies, and A. G. Yodh, "Diffuse optical monitoring of hemodynamic changes in piglet brain with closed head injury," J. Biomed. Opt. **14**, 034015 (2009).
13. C. Zhou, "In vivo optical imaging and spectroscopy of cerebral hemodynamics," Ph. D. thesis, University of Pennsylvania (Philadelphia, 2007).
14. T. Durduran, R. Choe, W. B. Baker, and A. G. Yodh, "Diffuse optics for tissue monitoring and tomography," Rep. Prog. Phys. **73**, 076701 (2010).
15. G. Dietsche, M. Ninck, C. Ortolf, J. Li, F. Jaillon, and T. Gisler, "Fiber-based multi-speckle detection for time-resolved diffusing-wave spectroscopy: Characterization and application to blood flow detection in deep tissue," Appl. Opt. **46**, 8506–8514 (2007).
16. D. A. Boas, "Diffuse photon probes of structural and dynamical properties of turbid media: Theory and biomedical applications," Ph. D. thesis, University of Pennsylvania (Philadelphia, 1996).
17. M. R. Arnfield, R. P. Mathew, J. Tulip, and M. S. McPhee, "Analysis of tissue optical coefficients using an approximate equation valid for comparable absorption and scattering," Phys. Med. Biol. **37**, 1219 (1992).
18. F. P. Bolin, L. E. Preuss, R. C. Taylor, and R. J. Ference, "Refractive index of some mammalian tissues using a fiber optic cladding method," Appl. Opt. **28**, 2297–2303 (1989).
19. R. C. Haskell, L. O. Svaasand, T.-T. Tsay, T.-C. Feng, M. S. McAdams, and B. J. Tromberg, "Boundary conditions for the diffusion equation in radiative transfer," J. Opt. Soc. Am. A **11**, 2727–2741 (1994).
20. D. A. Weitz and D. J. Pine, "Diffusing-wave spectroscopy," in "Dynamic Light Scattering. The method and some applications," , W. Brown, ed. (Clarendon Press, Oxford, 1993), pp. 652–720.
21. M. Friebel, A. Roggan, G. Müller, and M. Meinke, "Determination of optical properties of human blood in the spectral range 250 to 1100 nm using Monte-Carlo simulations with hematocrit-dependent effective scattering phase functions," J. Biomed. Opt. **11**, 034021 (2006).
22. M. Belau, M. Ninck, G. Hering, L. Spinelli, D. Contini, A. Torricelli, and T. Gisler, "Non-invasive observation of skeletal muscle contraction using near-infrared time-resolved reflectance and diffusing-wave spectroscopy," J. Biomed. Opt. **15**, 057007 (2010).
23. H. L. Goldsmith and J. C. Marlow, "Flow behavior of erythrocytes. II. Particle motions in concentrated suspensions of ghost cells," J. Colloid Interface Sci. **71**, 383–407 (1979).

Introduction

Microvascular blood flow is, apart from oxygen saturation, an essential parameter determining the efficiency of oxygen supply to tissue, bearing considerable relevance to therapy monitoring and planning in, e.g., photodynamic therapy of tumors, neonatology or neurointensive care. Traditional methods for non-invasively measuring microvascular blood flow such as PET, Xe CT or X-ray angiography offer high spatial resolution and sensitivity, but involve external contrast agents and radiation dose concerns and cannot be used at the bedside, which is a major difficulty for situations where chronic monitoring is required, such as in neurointensive care or in neonatology. Near-infrared diffusing-wave spectroscopy (DWS; also called diffuse correlation spectroscopy, DCS) has recently been introduced as a new technique for non-invasive detection of blood flow in deep tissue without the need for exogenous contrast agents. DWS is the extension of quasi-elastic light scattering to highly turbid media [1, 2] and analyzes the

#136026 - $15.00 USD Received 1 Oct 2010; revised 12 Nov 2010; accepted 20 Nov 2010; published 29 Nov 2010

temporal intensity fluctuations of multiply scattered light which arise from microscopic motions of scatterers within tissue, e.g. due to blood flow or tissue shearing. In contrast to the laser Doppler technique, DWS allows to probe tissue at depths of several centimeters, providing e. g. non-invasive access to brain function through the intact scalp and skull [3, 4]. Functional DWS signals from the human brain during motor or visual cognitive tasks show accelerated dynamics [3, 4, 5, 6, 7] which is explained by increased blood flow in the activated cortical areas induced by vasodilation. Comparisons with direct measurements of relative blood flow rates using arterial spin label (ASL) MRI in human skeletal muscle [8], human and rat brain [9, 10], Xe CT in the human brain [11] and fluorescent microspheres in the piglet brain [12] show high correlations (correlation coefficients 0.64–0.86) with relative flow indices derived from DWS data. However, the microscopic origin of the perfusion-related DWS signal has remained unclear so far. The temporal autocorrelation function $g^{(1)}(\tau)$ of the scattered light field from perfused tissue is found to be described by diffusion rather than by ballistic motion expected for flow-driven erythrocytes [4, 13, 14]. The analysis of *in vivo* DWS data from microvascular tissue is complicated by the simultaneous presence of erythrocyte motions and shear within extravascular tissue due to the pressure waves propagating from the heart through the arterial tree; indeed, high-resolution DWS data measured *in vivo* with a multi-speckle detection show that the field autocorrelation functions at the systole and at the diastole differ in their shape [15], suggesting that intravascular erythrocyte motions and extravascular tissue shearing contribute differently to the DWS signal, with weights varying within the pulsation cycle. However, experimental data quantifying the contributions of blood flow and extravascular tissue shearing under controlled conditions have not been available so far.

In this publication we present DWS data from porcine kidney which is artificially perfused *ex vivo* with controlled flow rate and pressure. Field autocorrelation functions measured on the renal cortex are described by diffusive dynamics for constant flow, with a particle diffusion coefficient scaling linearly with the volume flow rate Q. Dynamic contrast variation, i.e., replacing blood by non-scattering saline solution, reveals a small residual background dynamics within the extravascular tissue which is independent of flow rate. For pulsatile flow scatterer dynamics is approximately diffusive, with a time-dependent effective diffusion coefficient whose modulation bears the signatures of flow in the presence of blood, and of shear motions for the blood-free kidney.

1. Experimental

A fresh kidney of an adult pig, obtained from the Konstanz slaughterhouse, was prepared by removing surrounding tissue. After removing residual blood by repeated perfusion with a 0.15 M NaCl solution through the Arteria renalis, the vascular volume was filled with a solution of 3000 units/ℓ heparin (Braun) in 0.15 M NaCl. During the experiment, the kidney was artificially perfused using a home-built perfusor driven by a linear motor (controller: LinMot E1100-RS; stator: LinMot PS01-37x120-C) (see Fig. 1). Perfusion was controlled by operating the motor either at constant velocity or at a sinusoidally varying velocity $v_{\mathrm{m}}(t) = v_{\mathrm{m},0} + \delta v \sin(2\pi f_0 t)$ at a frequency $f_0 = 1\,\mathrm{Hz}$. The injected volume was calculated from the position information provided by the perfusor controller unit. Arterial pressure p_{a} was measured at the entrance of the Arteria renalis with a piezoelectric sensor (Honeywell 24PCBFA6G). Relative variations of pressure and flow rate were less than 0.17% and 1.5%, respectively. Experiments with two different perfusion media were carried out: (i) a 0.15 M NaCl solution and (ii) fresh porcine blood at a dilution of 9% of the physiological hematocrit suspended in a solution of 0.13 M NaCl and 0.01 M sodium citrate. Vascular patency was confirmed by x-ray angiography.

DWS experiments were performed using an external-cavity diode laser (Toptica TA-100) operating at a wavelength $\lambda = 802\,\mathrm{nm}$ as a source. Its light was guided onto the kidney sur-

#136026 - $15.00 USD Received 1 Oct 2010; revised 12 Nov 2010; accepted 20 Nov 2010; published 29 Nov 2010

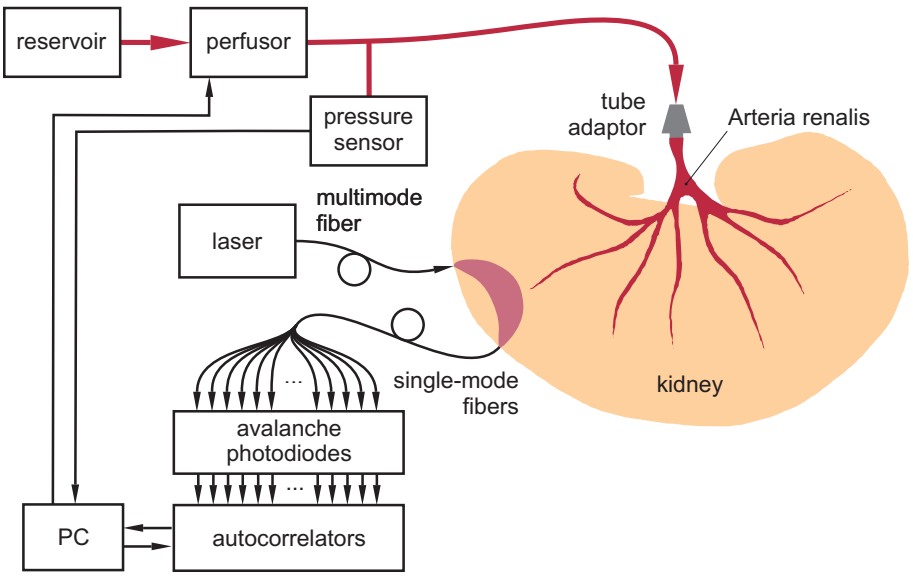

Fig. 1. Schematic experimental setup. The kidney, which is fixed in a rigid construction in order to minimize motion artefacts, is perfused by a computer-controlled perfusor consisting of a syringe driven by a linear motor at controlled velocity. The DWS sensor is placed on the Extremitas inferior and probes approximately the banana-shaped volume marked in pink. Injected fluid is drained through the vena renalis (not shown).

face by a multimode optical fiber. Laser powers were 51 mW and 100 mW over a tissue area of about 12 mm^2 for the experiments with saline buffer and with diluted blood, respectively. The DWS sensor, consisting of a bundle of 31 single-mode receiver fibers (Schäfter+Kirchhoff SMC-780; nominal cut-off wavelength 780 nm, mode field diameter 4.7 μm, numerical aperture 0.13) was placed at a distance $\rho = 18$ mm from the source at the Extremitas inferior. Light from each of the receiver fibers was detected by an avalanche diode (Perkin-Elmer SPCM-AQ4C) whose TTL output is processed by a multichannel autocorrelator (correlator.com) (see [15] for details). In order to perform experiments in the presence of ambient light we equipped the fiber receiver with a bandpass filter (Semrock FF01-800/12-25) with 12 nm spectral width and 93 % transmission at the center wavelength 800 nm. Both for constant and for modulated flow the bundle-averaged field autocorrelation functions $g^{(1)}(\tau)$ were measured with an integration time $T = 26.2$ ms; this is short enough that the scatterer dynamics can be considered stationary at the pulsation frequency $f_0 = 1$ Hz. The average photon count rate was between 24 kHz and 96 kHz per fiber.

To characterize the nature of the motions giving rise to the decay of $g^{(1)}(\tau)$, we computed the mean square phase fluctuation $\langle \Delta\varphi^2(\tau)\rangle$ for a single scattering event by numerical inversion of the expression for $g^{(1)}(\tau)$ for a semi-infinite, optically and dynamically homogeneous medium and point source-point receiver geometry [16],

$$g^{(1)}(\tau) = \frac{1}{R(\rho)}\left[\frac{\exp\left(-\alpha(\tau)\, r_1\right)}{r_1} - \frac{\exp\left(-\alpha(\tau)\, r_2\right)}{r_2}\right] \tag{1}$$

for the dynamic absorption coefficient $\alpha(\tau) = \left(3\mu_s'\mu_a + \frac{3}{2}\mu_s'^2\langle\Delta\varphi^2(\tau)\rangle\right)^{1/2}$. Here $R(\rho) = \exp\left(-\alpha(0)\, r_1\right)/r_1 - \exp\left(-\alpha(0)\, r_2\right)/r_2$ is proportional to the average diffuse reflectance at the source-receiver distance ρ. The quantities $r_1 = \left(\rho^2 + z_0^2\right)^{1/2}$ and $r_2 = \left(\rho^2 + (z_0 + 2z_e)^2\right)^{1/2}$

#136026 - $15.00 USD Received 1 Oct 2010; revised 12 Nov 2010; accepted 20 Nov 2010; published 29 Nov 2010

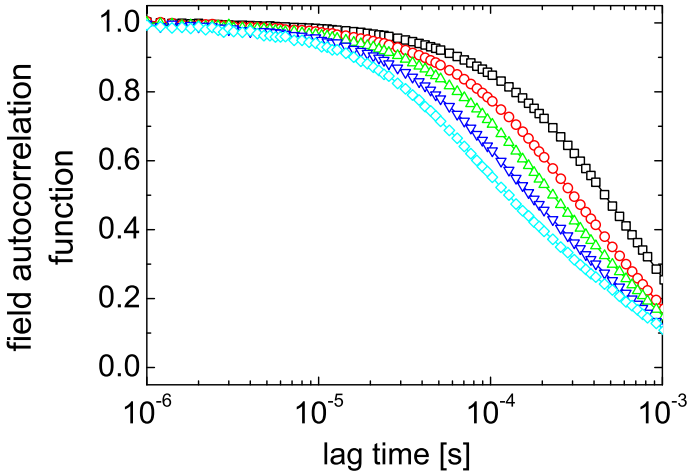

Fig. 2. Field autocorrelation functions $g^{(1)}(\tau)$ as a function of lag time τ measured at the Extremitas inferior of the porcine kidney during constant perfusion with diluted blood for flow rates $Q = 0.6\,\mathrm{m}\ell/\mathrm{s}$ (□), $1.2\,\mathrm{m}\ell/\mathrm{s}$ (○), $1.8\,\mathrm{m}\ell/\mathrm{s}$ (△), $2.4\,\mathrm{m}\ell/\mathrm{s}$ (▽) and $3.1\,\mathrm{m}\ell/\mathrm{s}$ (◇). Source-receiver distance is $\rho = 18\,\mathrm{mm}$. For better visibility of the flow dependence, data for lag times $\tau > 1\,\mathrm{ms}$ are suppressed. Data are averages over 1908 autocorrelation functions each measured with an acquisition time of 26.2 ms, corresponding to a total experiment duration of 50 s for each flow rate. Standard deviations of $g^{(1)}(\tau)$ are smaller than 2×10^{-3}.

are related to the depth $z_0 = 1/\mu_s'$ of the effective diffuse light source. For the reduced scattering and absorption coefficients we used values $\mu_s' = 5.4\,\mathrm{cm}^{-1}$ and $\mu_a = 0.5\,\mathrm{cm}^{-1}$, respectively [17]. With a tissue refractive index $n \approx 1.4$ [18], we estimate the value for the extrapolation length $z_e \approx 1.9/\mu_s'$ [19]. For independent scatterers $\langle \Delta\varphi^2(\tau) \rangle$ is related to the scatterer mean square displacement $\langle \Delta r^2(\tau) \rangle$ by $\langle \Delta\varphi^2(\tau) \rangle = 2k_0^2/3 \langle \Delta r^2(\tau) \rangle$, where $k_0 = 2\pi n/\lambda$ is the wavevector in the medium [20]. Allowing for variations of z_e in the range $[1.5/\mu_s', 2.5/\mu_s']$ leads to relative changes of the retrieved $\langle \Delta\varphi^2(\tau) \rangle$ of no more than 2.2 %.

For the experiments with modulated flow, DWS autocorrelation functions measured at times $t, t + 1/f_0, t + 2/f_0, \ldots$, of several pulsation cycles were averaged, from which the time-dependent mean square phase fluctuation $\langle \Delta\varphi^2(\tau, t') \rangle$ as a function of lag time τ and phase $t' = t \bmod (1/f_0)$ were computed as described above.

2. Results

2.1. *Constant flow*

Field autocorrelation functions $g^{(1)}(\tau)$ from kidneys perfused with diluted blood are very reproducible over periods of typically 50 s, reflecting the stability of the flow, and decay within about $460\,\mu\mathrm{s}$ for the lowest flow rate $Q = 0.6\,\mathrm{m}\ell/\mathrm{s}$; increasing the flow rate strongly accelerates the decay (see Fig. 2).

As shown in Fig. 3, mean square phase fluctuations $\langle \Delta\varphi^2(\tau) \rangle$ show linear scaling with lag time between about $10^{-5}\,\mathrm{s}$ and $10^{-4}\,\mathrm{s}$, indicating diffusive erythrocyte dynamics characterized by a mean square displacement $\langle \Delta r^2(\tau) \rangle = 3\langle \Delta\varphi^2(\tau) \rangle / \left(2k_0^2\right) = 6D\tau$ and a diffusion coefficient D. This behavior contradicts the ballistic scaling $\langle \Delta\varphi^2(\tau) \rangle \sim \langle v^2 \rangle \tau^2$ expected for random flow of uncorrelated scatterers with mean square velocity $\langle v^2 \rangle$. Plotting D vs. the volume flow

#136026 - $15.00 USD Received 1 Oct 2010; revised 12 Nov 2010; accepted 20 Nov 2010; published 29 Nov 2010

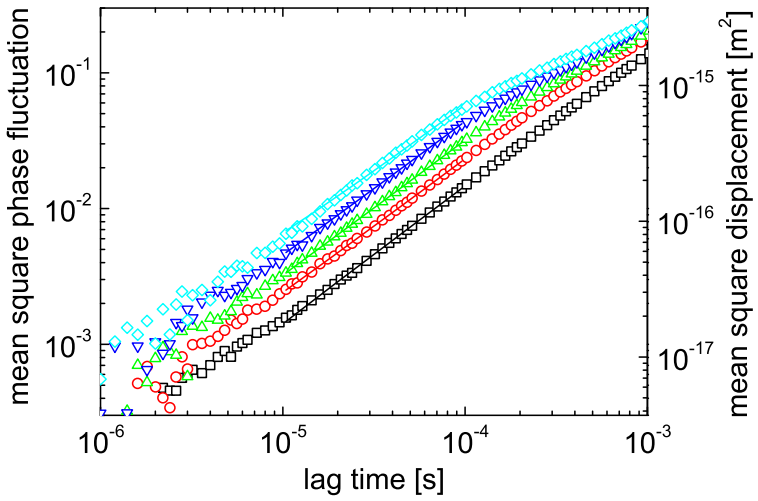

Fig. 3. Mean square phase fluctuation $\langle\Delta\varphi^2(\tau)\rangle$ and mean square displacement $\langle\Delta r^2(\tau)\rangle$ in porcine kidney perfused with 9 % blood as a function of lag time τ, for flow rates $Q =$ 0.6 mℓ/s (□), 1.2 mℓ/s (○), 1.8 mℓ/s (△), 2.4 mℓ/s (▽) and 3.1 mℓ/s (◇). Linear least-squares fits of the function $a_0 + a_1\tau$ to the data for lag times $10^{-5}\,\text{s} \le \tau \le 10^{-4}\,\text{s}$ are shown as lines.

rate in the range $0.6\,\text{m}\ell/\text{s} \le Q \le 3.1\,\text{m}\ell/\text{s}$ shows a linear scaling $D(Q) \sim Q$ (see Fig. 4). For the blood-filled kidney in the absence of flow the intensity autocorrelation function decays within about 1 ms; the low intercept of about 1.35 indicates substantial static scattering from extravascular tissue, precluding quantitative determination of $\langle\Delta\varphi^2(\tau)\rangle$.

When the kidney is perfused with the saline solution, the field autocorrelation function $g^{(1)}(\tau)$ is observed to decay on a time scale of about 700 μs which is by a factor of 1.8 longer than the slowest decay in the presence of blood (see Fig. 5), but shorter than the decay time for the blood-filled kidney without flow. In contrast to the data for the blood-perfused kidney, the DWS autocorrelation functions for saline perfusion depend only very weakly on flow rate. The short integration time of 26.2 ms introduces normalization errors and distortions at large τ for such slowly decaying autocorrelation functions, making meaningful determination of $\langle\Delta\varphi^2(\tau)\rangle$ difficult.

2.2. Pulsatile flow

For the pulsatile flow realized by sinusoidally modulating the syringe velocity, we obtain nearly sinusoidal modulations of the arterial pressure for perfusion with both diluted blood and saline solution (see Fig. 6a). For perfusion with saline solution, the flow rate $Q(t')$ shows a symmetric, nearly sinusoidal modulation; in contrast, $Q(t')$ in the presence of blood is strongly asymmetric (see Fig. 6b). The cycle-averaged pressure $\langle p_\text{a}\rangle_\text{c}$ shows a linear scaling with the cycle-averaged flow rate $\langle Q\rangle_\text{c}$ both for blood and saline perfusion, with effective vascular resistances $\langle p_\text{a}\rangle_\text{c}/\langle Q\rangle_\text{c}$ very similar to the ones for constant flow (data not shown).

Mean square phase fluctuations $\langle\Delta\varphi^2(\tau,t')\rangle$ depend, both for perfusion with blood and with saline solution, on the phase t' within the pulsation cycle (see Fig. 7). In contrast to the clear linear scaling with τ for constant flow, $\langle\Delta\varphi^2(\tau,t')\rangle$ measured at different t' show a relatively complex behavior and can in general not be superimposed by rescaling lag time, corroborating

#136026 - $15.00 USD Received 1 Oct 2010; revised 12 Nov 2010; accepted 20 Nov 2010; published 29 Nov 2010

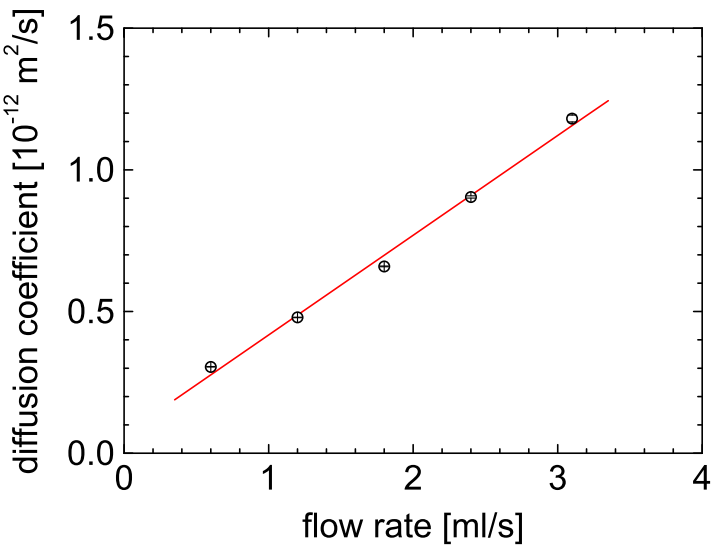

Fig. 4. Particle diffusion coefficient D of the blood-perfused kidney as a function of volume flow rate Q. The full line is a linear least-squares fit to the data. Values for intercept and slope are $(6.5 \pm 3.3) \times 10^{-14}\,\mathrm{m}^2/\mathrm{s}$ and $(3.5 \pm 0.16) \times 10^{-13}\,\mathrm{m}^2/\mathrm{m}\ell$, respectively. Error bars denote the standard deviation of the residuals of the fit to $\langle \Delta\varphi^2(\tau) \rangle$.

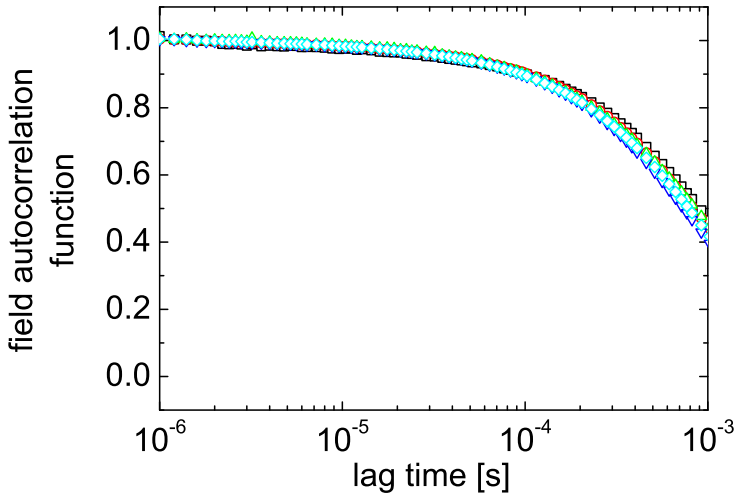

Fig. 5. Field autocorrelation functions $g^{(1)}(\tau)$ as a function of lag time τ measured on the kidney during constant perfusion with saline solution for flow rates $Q = 0.6\,\mathrm{m}\ell/\mathrm{s}$ (□), $1.2\,\mathrm{m}\ell/\mathrm{s}$ (○), $1.8\,\mathrm{m}\ell/\mathrm{s}$ (△), $2.4\,\mathrm{m}\ell/\mathrm{s}$ (▽) and $3.1\,\mathrm{m}\ell/\mathrm{s}$ (◇). $g^{(1)}(\tau)$ was calculated from measured $g^{(2)}(\tau)$ using coherence factors $\beta \approx 0.45$ determined from a fit of $g^{(2)}(\tau) - 1$ to $\beta + a_1\tau + a_2\tau^2$.

#136026 - $15.00 USD Received 1 Oct 2010; revised 12 Nov 2010; accepted 20 Nov 2010; published 29 Nov 2010

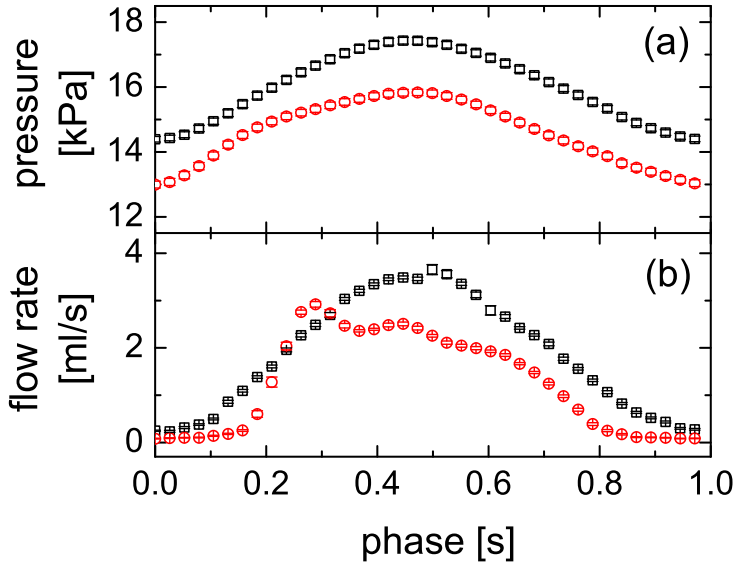

Fig. 6. (a) Arterial pressure $p_a(t')$ and (b) flow rate $Q(t')$ as a function of phase t' within the pulsation cycle. Circles: diluted blood; squares: saline solution. Data are averages over 31 and 16 measurements for diluted blood and for saline solutions, respectively, each with an integration time of 26.2 ms.

the *in vivo* observation on the human index finger reported in [15].

In order to characterize the evolution of the scatterer dynamics over the pulsation cycle by a single parameter, we calculate the effective diffusion coefficient $D_{\mathrm{eff}}(t')$ by a linear least-squares fit of the function $4k_0^2 D_{\mathrm{eff}}(t')\tau$ to the measured $\langle \Delta\varphi^2(\tau,t')\rangle$ in the lag time window $50\,\mu\mathrm{s} \le \tau \le 500\,\mu\mathrm{s}$. However, it should be noted that a super-diffusive scaling $\langle \Delta\varphi^2(\tau,t)\rangle \sim a(t')\tau^{\kappa(t')}$ with a phase-dependent exponent $\kappa(t')$ fits the data slightly better. However, as the physical meanings of the parameters a and κ are not evident, we only discuss the single parameter $D_{\mathrm{eff}}(t')$ in the following. In the presence of blood, $D_{\mathrm{eff}}(t')$ varies approximately sinusoidally around an average value which increases with mean arterial pressure (see Fig. 8). For the saline-perfused kidney, the effective diffusion coefficient in the saline-perfused kidney shows a qualitatively and quantitatively different behavior with 2 maxima during the pulsation cycle and a significantly reduced average value and modulation.

Discussion

While replacing blood by non-scattering saline solution provides access to the dynamics of the extravascular tissue, a quantitative understanding of the resulting changes in the DWS signals requires an estimation of the changes in the optical properties entailed by this procedure. We estimate the optical properties of the blood-free kidney with the expression $\mu_s' = (1-\phi_v)\mu_{s,ev}'$, where $\phi_v \approx 0.07$ is the average vascular volume fraction determined from our vascular corrosion casts; the value of the reduced scattering coefficient of the bulk extravascular tissue, $\mu_{s,ev}'$, is estimated using the expression $\mu_{s,ev}' = \mu_s' - \phi_v\mu_{s,v}'/(1-\phi_v) \approx 4.3\,\mathrm{cm}^{-1}$. Here, $\mu_s' = 5.4\,\mathrm{cm}^{-1}$ is the literature value of the reduced scattering coefficient of the kidney perfused with full blood [17]; for the reduced scattering coefficient $\mu_{s,v}'$ of the vascular compartment, we have assumed

#136026 - $15.00 USD Received 1 Oct 2010; revised 12 Nov 2010; accepted 20 Nov 2010; published 29 Nov 2010

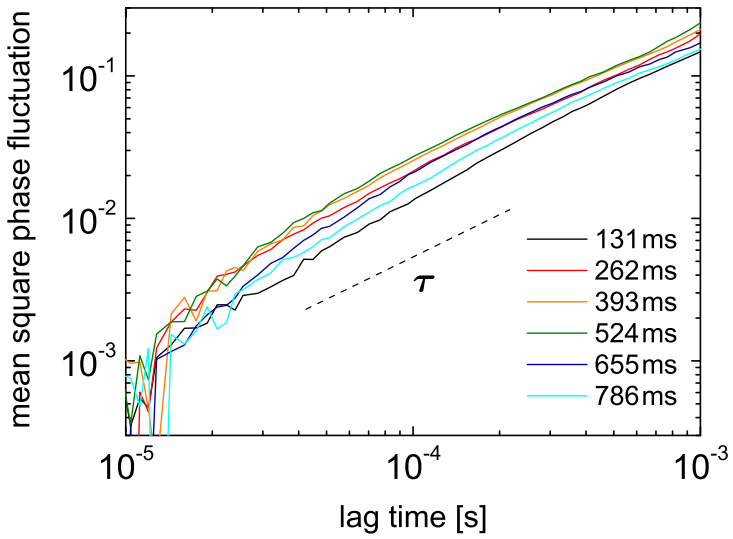

Fig. 7. Mean square phase fluctuation $\langle \Delta\varphi^2(\tau,t')\rangle$ of the blood-perfused kidney as a function of lag time τ measured at different phases t' in the pulsation cycle. Average flow rate $Q = 1.2\,\mathrm{m}\ell/\mathrm{s}$. The dashed line denotes, for comparison, the diffusive scaling $\langle \Delta\varphi^2(\tau)\rangle \sim \tau$ observed for constant flow. Data are averages over 31 measurements each with an integration time of 26.2 ms.

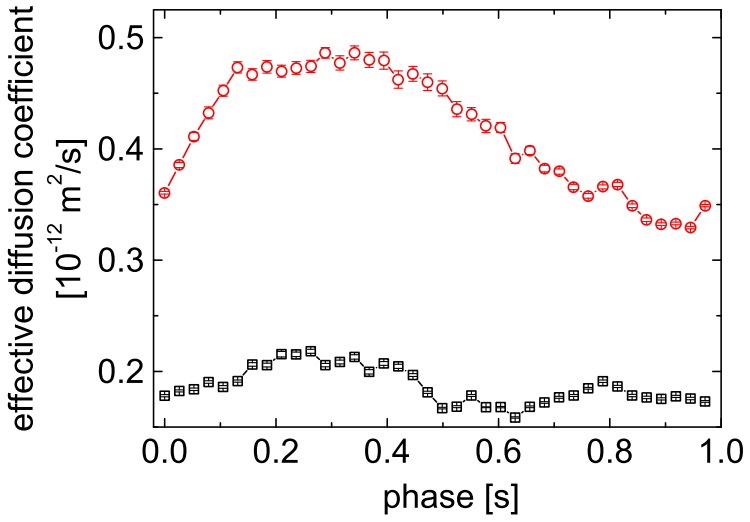

Fig. 8. Effective diffusion coefficient $D_{\mathrm{eff}}(t')$ as a function of phase t' within the pulsation cycle. Circles: diluted blood at average arterial pressure 14.6 kPa and average flow rate $1.25\,\mathrm{m}\ell/\mathrm{s}$. Squares: saline solution at average arterial pressure 16 kPa and average flow rate $1.86\,\mathrm{m}\ell/\mathrm{s}$.

#136026 - $15.00 USD Received 1 Oct 2010; revised 12 Nov 2010; accepted 20 Nov 2010; published 29 Nov 2010

a value of $20\,\mathrm{cm}^{-1}$ reported for human blood at full hematocrit [21].

The blood-free kidney is thus estimated to have a reduced scattering coefficient $(1-\phi_\mathrm{v})\mu'_{\mathrm{s,ev}} \approx 4.0\,\mathrm{cm}^{-1}$, practically identical with the estimate $\mu'_\mathrm{s} \approx 4.1\,\mathrm{cm}^{-1}$ for the kidney perfused with diluted blood. Diffusion coefficients shown in Figs. 4 and 8 are thus likely to be underestimated by the same factor $(5.4/4.1)^2 \approx 1.7$ when determined using the literature value for the reduced scattering coefficient. Clearly, optical properties measured *in situ* taking into account sample-to-sample variations should allow for a more quantitative determination of diffusion coefficients.

Our calculation of the mean square phase fluctuation per scattering event, $\langle \Delta\varphi^2(\tau)\rangle$, and the erythrocyte diffusion coefficient D using the bulk values for μ'_s and μ_a assumes that all the scatterers are mobile. However, this approach is likely to underestimate the actual diffusion coefficient: despite its high contribution to the total μ'_s, the dynamics of the extravascular tissue is very weak compared to the one of the vascular compartment (see Fig. 5). An upper bound for the intravascular diffusion coefficient can be estimated by assuming the extravascular tissue to be completely static. Then the actual diffusion coefficient D_v of the vascular compartment is related to the measured D by $D_\mathrm{v} = D/f$, where f is the fraction of scattering events a photon experiences with mobile scatterers. For values of the reduced scattering coefficient μ'_s of the perfused kidney between $4.1\,\mathrm{cm}^{-1}$ and $5.4\,\mathrm{cm}^{-1}$ we estimate that the fraction of scattering events by erythrocytes, $\phi_\mathrm{v}\mu'_{\mathrm{s,v}}/\mu'_\mathrm{s}$, is between 3 % and 4.5 %, resulting in D_v being between 30 and 40 times larger than the measured D.

While the linear scaling of the measured diffusion coefficient D with flow rate is suggestive of a direct linear relationship between actual, intravascular diffusion coefficient and Q, it should be kept in mind that for low pressures an increase in flow may be accompanied by a substantial increase in vascular volume, leading, via the increase in f, to an increased measured diffusion coefficient which reflects the vascular compliance, but not the actual flow rate. This effect is expected to be important for low arterial pressures and high vascular compliance and could be the origin for reported deviations between DWS flow indices and flow rates measured by methods such as ASL MRI. At high pressures, the vascular volume will saturate due to the finite extensibility of the vascular walls. Indeed, we observe that average photon count rates vary significantly only at the lowest arterial pressure, while they are constant to within less than 1 % for the highest pressures and flow rates. Model calculations show that these reflectance changes correspond to pressure-induced variations of f which are far too small to account for the large variations of the measured diffusion coefficient for flow rates $Q \gtrsim 0.6\,\mathrm{m}\ell/\mathrm{s}$.

Accounting for these optical effects we estimate that the actual diffusion coefficients for pulsatile flow shown in Fig. 8 are by a factor of 60–80 larger than the ones in the saline-perfused kidney, indicating that for flow rates within the physiological range the major contribution to the DWS signal is indeed due to erythrocyte motions, as suggested by the earlier *in vivo* validation experiments.

This conclusion is also supported by the qualitatively different temporal evolution of $D_\mathrm{eff}(t')$ during the pulsation cycle. As shown in Fig. 9, the spectrum (Fourier transform) of $D_\mathrm{eff}(t)$ shows a strong component at $f = 2f_0$ for the saline-perfused kidney, which is the hallmark of shear dynamics, as was recently observed in time-resolved DWS experiments on contracting skeletal muscles [22]. For the blood-perfused kidney, such a frequency-doubled component is strongly attenuated in comparison with the fundamental mode at 1 Hz despite the highly anharmonic flow rate observed at the entrance of the vascular system. Assuming that the low-pass filter property of the vascular tree results in nearly sinusoidal flow within the renal cortex, we expect, extending the linear flow rate scaling of D in the constant-flow regime to pulsatile flow, a modulation of $D(t')$ with f_0, in line with the observed behavior.

The approximately linear lag time scaling of the mean square phase fluctuations $\langle \Delta\varphi^2(\tau,t')\rangle$

#136026 - $15.00 USD Received 1 Oct 2010; revised 12 Nov 2010; accepted 20 Nov 2010; published 29 Nov 2010

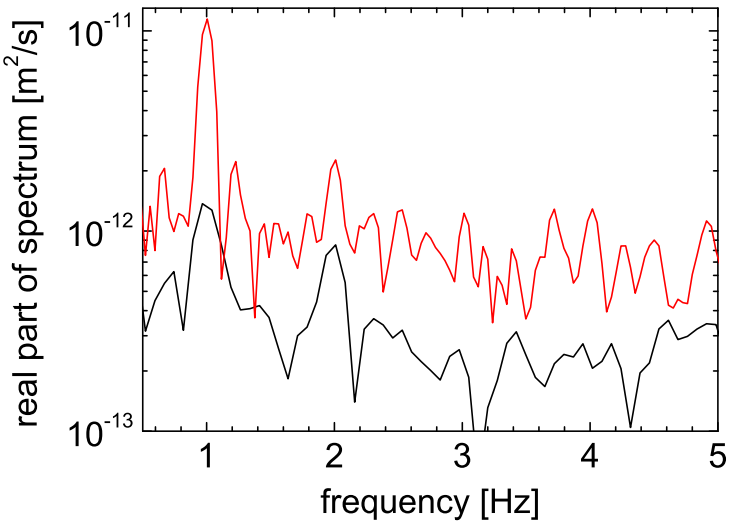

Fig. 9. Real part of the spectrum of the effective diffusion coefficient $D_{\mathrm{eff}}(t)$ for the kidney perfused with blood (red) and with saline buffer (black), as a function of frequency f. Note the strong peak at the pulsation frequency $f_0 = 1\,\mathrm{Hz}$ and the marked second harmonic at 2 Hz for the saline-perfused kidney indicating the contributions of extravascular tissue shearing.

measured at different phases of the pulsation cycle clearly shows that the deviations of the field autocorrelation function from the expected ballistic behavior observed *in vivo* [4, 13, 14] does not arise from time-averaging of $g^{(1)}(\tau,t)$ over integration times longer than the pulse cycle time $1/f_0$. To date, all available *in vivo* DWS data were measured non- or semi-invasively, leaving the possibility that the diffusive dynamics obtained by analysis of $g^{(1)}(\tau)$ with a homogeneous semi-infinite model could arise from the neglect of optical and dynamic heterogeneity. However, the analysis of *in vivo* DWS data from the human motor cortex with a 3-layer model showed that even by accounting for different optical and dynamical properties in the scalp, skull and cortex, data could not be described by ballistic erythrocyte dynamics expected for random flow [4]. Such multi-layer models are based on the assumption that the diffusion approximation holds within the individual, optically homogeneous, layers. For values of μ_s' between $4.0\,\mathrm{cm}^{-1}$ and $5.4\,\mathrm{cm}^{-1}$ and μ_a between $0.3\,\mathrm{cm}^{-1}$ and $0.5\,\mathrm{cm}^{-1}$ and using the diffusion approximation for the source-receiver distance $\rho = 18\,\mathrm{mm}$ we estimate that the detected photons undergo between 13 and 18 scattering events for the blood-perfused and the blood-free kidney. While this hints at the limited validity of the diffusion approximation in particular for long lag times and short photon paths, it is unlikely to be fully responsible for the linear lag time scaling of $\langle\Delta\varphi^2(\tau)\rangle$ at the relatively short τ observed under constant flow conditions. Rather, it might reflect diffusive erythrocyte dynamics brought about by collisions with other erythrocytes or the vessel walls. Indeed, particle tracking experiments by Goldsmith and Marlow [23] revealed diffusive erythrocyte dynamics in the direction perpendicular to the flow, with a diffusion coefficient approximately linear in the average shear rate. As the shear rate scales with Q for the laminar flow conditions realized in microvasculature, the collision mechanism could also explain the linear scaling of the diffusion coefficient with Q observed in our constant-flow experiments.

#136026 - $15.00 USD Received 1 Oct 2010; revised 12 Nov 2010; accepted 20 Nov 2010; published 29 Nov 2010

Conclusions

The dynamic contrast variation method introduced here allows to disentangle the effects of extravascular shearing and erythrocyte dynamics on DWS signals from perfused tissue. While our experiments were focussed on the renal cortex as a model system for microvascular tissue, we expect that our results can be transferred to other tissues with similar vascular architecture, such as the cerebral cortex. Together with measurements of tissue optical properties this method could provide the basis of all-optical, non-invasive measurements of absolute microvascular blood flow rates.

Acknowledgments

We thank A. Beck for x-ray angiography, and and Otto Müller GmbH for providing the kidneys. This work was funded by the Deutsche Forschungsgemeinschaft and the Center for Applied Photonics (CAP) Konstanz.

#136026 - $15.00 USD Received 1 Oct 2010; revised 12 Nov 2010; accepted 20 Nov 2010; published 29 Nov 2010